JMEPEG (2014) 23:3831–3841
DOI: 10.1007/s11665-014-1193-3

1059-9495/$19.00

Effects of Solution Heat Treatment on Microstructure and Mechanical Properties of the Mg-4.5Zn-4.5Sn-2Al-0.6Sr Alloy

Guanghao Zhang, Jihua Chen, Hongge Yan, and Bin Su

(Submitted January 27, 2014; in revised form July 20, 2014; published online August 13, 2014)

Microstructure and mechanical properties of the Mg-4.5Zn-4.5Sn-2Al-0.6Sr alloy are investigated both in the as-cast condition and after the different three-step solution heat treatments (a solution heat treatment of 310 °C × 4 h + 340 °C × 28 h followed by a high-temperature solution treatment) to explore the optimal solution treatment cycle. The as-cast alloy contains a microstructure consisting of the α-Mg matrix, Mg_2Sn, $Mg_{51}Zn_{20}$, $Mg_{32}(Al, Zn)_{49}$, and MgSnSr phases. After the solution heat treatment, all the $Mg_{51}Zn_{20}$, the $Mg_{32}(Al, Zn)_{49}$ phases, and most of the Mg_2Sn phase are dissolved into the matrix, only the MgSnSr phase and a minority of the Mg_2Sn phase are remained in the granular form or the fine dot-like. The volume fraction of the residual second phases decreases from 5.61 to 1.84% with the increasing solution time from 0 to 4 h at 420 °C and it decreases from 2.9 to 0.4% with the increasing solution temperature from 420 to 480 °C for 2 h. The alloy that experiences the solution treatment of 310 °C × 4 h + 340 °C × 28 h + 460 °C × 2 h exhibits the highest strength and the best plasticity among all the solution-treated alloys. Therefore, the optimal solution treatment is 310 °C × 4 h + 340 °C × 28 h + 460 °C × 2 h. The residual second phases in the alloy that experiences the optimal solution treatment are confirmed to be the Mg_2Sn phase and the MgSnSr phase which are related to their relatively high thermal stability. The ultimate tensile strength and the elongation to rupture of the as-solutionized alloy are 238 MPa and 12%, respectively, about 25 MPa and 2.4% higher than the counterparts of the as-cast alloy.

Keywords mechanical properties, Mg-Zn-Sn alloy, microstructure, solution heat treatment, solution strengthening

1. Introduction

Conventional magnesium alloys exhibit relatively low strength, poor creep resistance, and inferior plasticity due to the intrinsic hcp structure and cannot be used for the manufacture of key structural components (Ref 1). Therefore, it is of great significance to develop novel magnesium alloys with high strength and good toughness. In the recent years, more and more attention has been paid to the Mg-Zn-Sn system whose strengthening mechanism is mainly connected with the formation of two precipitates, i.e., MgZn and Mg_2Sn. It is reported that the Mg-Zn-Sn alloy is a promising new heat-treatable alloy (Ref 2), a promising candidate for future commercial applications at elevated temperatures (Ref 3), and suitable for extrusion to give a high strength (Ref 4).

Up to now, most studies are focused on improving microstructure and mechanical properties of the Mg-Zn-Sn system by alloying such as RE (Ref 5) and Al (Ref 3, 6, 7) and micro-alloying such as Ca (Ref 8, 9) and Y (Ref 10). Moreover, several studies are attempted to develop the high-strength heat-treatable wrought magnesium alloys based on the Mg-Zn-Sn alloy system (Ref 4, 11, 12). The precipitation sequence of the Mg-Zn-Sn alloy system has been cleared and the effects of minor alloying on its precipitation behaviors have been widely studied. However, the formation and the evolution of the α-Mg supersaturated solid solution with minor Sr addition in this alloy system have not been well understood. Determining the optimal solution treatment conditions is a major consideration in the fabrication of the high-performance heat-treatable Mg-Zn-Sn alloys. Therefore, it is of great theoretical and practical significance to investigate the diffusion in the Mg-Zn-Sn alloys and the morphology change of the second phases during solution heat treatment.

Our previous work shows that the alloy with the Zn/Sn mass ratio of 1 exhibits a fairly good roll forming ability and much better mechanical properties among the Mg-*x*Zn-*y*Sn-2Al-0.2Ca ($x + y = 9$ wt.%) alloys (Ref 13). In addition, minor Sr addition can effectively refine grains, dendrites, and grain-boundary compounds, and these effects are more obvious with a higher Sr addition in the Mg-4.5Zn-4.5Sn-2Al-based alloys (Ref 14). Therefore, the main goal of the current study is to report the effects of the three-step solution heat treatment on the microstructure and mechanical properties of the Mg-4.5Zn-4.5Sn-2Al-0.6Sr alloy.

2. Experimental Details

The Mg-4.5%Zn-4.5%Sn-2%Al-0.6%Sr alloy is prepared in an electric resistance furnace with a mild steel crucible

Guanghao Zhang, Jihua Chen, Hongge Yan, and **Bin Su**, School of Materials Science and Engineering, Hunan University, Changsha 410082, P. R. China and Hunan Provincial Key Laboratory of Spray Deposition Technology & Application, Hunan University, Changsha 410082, P. R. China. Contact e-mail: jihuachen2005@163.com.

protected by the RJ-2 flux (37.1% KCl-43.2% $MgCl_2$-6.8% $BaCl_2$-4.8% CaF_2-6.6% [NaCl + $CaCl_2$]-1.3% water-insoluble—0.4% moisture). Commercially pure Mg, Al, Zn, Sn, Mn (99.9%) stuffs, and the Mg-9.2Sr master alloy are added to prepare these alloys. Mn is added to diminish the negative effect of the impurity Fe on corrosion resistance of the as-prepared alloys. The melt is purged at 720 °C for 10 min and held for 15 min at 760 °C so that homogenization of alloying elements and settlement of inclusions can be realized. Then, molten alloy is cast into a water-cooling steel mold ($100 \times 150 \times 20$ mm^3) at a casting temperature of 720 °C. The mold is made of the 0.45%C carbon steel.

Block specimens are cut from the as-cast plate and then the different three-step solution heat treatments (a solution heat treatment of 310 °C × 4 h + 340 °C × 28 h followed by a high-temperature solution treatment) are conducted respectively to ensure the complete dissolution of alloying elements in the α-Mg matrix. The solution treatments are conducted in the SR3 heat treatment furnace at the temperature control precision of ±2 °C, and the samples are covered with the mixture of sand and graphite. Water quenching is adopted. The as-cast and the as-solutionized microstructures are observed using a MM-6 metallographic microscope and a FEI QUANTA 200 scanning electron microscopy (SEM) after etching with a solution of 0.6-1.2 g picric acid, 2 mL acetic acid, 3 mL water, and 20 mL ethanol. The micro-compositional analysis of some certain phases is conducted on the FEI QUANTA 200 SEM and the JEM-2100 telescope electron microscopy (TEM), both equipped with the EDAX genesis xm-2 spectroscopy (EDS). Selected area electron diffraction (SAED) patterns of the certain phases are also recorded. The specimen for TEM observation is prepared by ion milling after mechanical polishing to the thickness of 90-120 μm. The volume fraction of the residual second phases is calculated using the Image-PropPlus 6.0 software on the basis of the optical images, which is bigger than the counterpart according to the SEM images. The overall phase constitutions of these alloys are analyzed by a D5000 x-ray diffraction instrument with Cu Kα and at a scanning rate of 0.01°/s. The heating curve of the as-cast alloy is recorded by a METZSCH differential scanning calorimeter (DSC)/differential thermal analysis (DTA) 404PC instrument at a scanning rate of 10 K/min. Microhardness testing is conducted on a MHV-2000 microhardness instrument with the load of 0.98 N and a holding time of 15 s. The as-cast plate and the alloy that experiences the different solution treatments are machined into flat tensile specimens with a gage section of $15 \times 4 \times 2$ mm^3. The tensile tests are performed on an Instron3369 tensile testing machine with an initial strain rate of 1.1×10^{-3} s^{-1} at room temperature. The ultimate tensile strength (UTS), the yield tensile strength (YTS), and the elongation to rupture (E_r) are averaged over three specimens.

3. Results

3.1 As-Cast Alloy

The XRD pattern of the as-cast Mg-4.5Zn-4.5Sn-2Al-0.6Sr alloy is shown in Fig. 1. It can be clearly seen that the as-cast alloy consists of five phases, i.e., α-Mg, Mg_2Sn, $Mg_{51}Zn_{20}$, $Mg_{32}(Al, Zn)_{49}$, and MgSnSr. However, the diffraction peaks corresponding to the MgSnSr phase are relatively weak, indicating that its content is rather low.

The SEM image of the as-cast alloy is shown in Fig. 2. Obviously, it exhibits a typical dendrite structure and is characteristic of divorced eutectics. A majority of divorced eutectics are isolated by scattered along grain boundaries in the granular form and a minority are in the bone-like. Our previous work shows that the Mg_2Sn, $Mg_{51}Zn_{20}$, and $Mg_{32}(Al, Zn)_{49}$ phases are formed mainly along grain boundaries, whereas the MgSnSr phase is possibly formed within grains (Ref 14).

The heating curve of the as-cast alloy recorded from ambient temperature to 540 °C is shown in Fig. 3. Three endo-thermal peaks are detected. The endo-thermal peak around 344 °C corresponds to the melting of the non-equilibrium eutectic. According to Ghosh et al. (Ref 15), a ternary eutectic transformation i.e., L → α-Mg + $Mg_{51}Zn_{20}$ + Mg_2Sn can occur at 342.3 °C when the composition of the liquid phase approaches to 71.32 at.%Mg, 0.25 at.%Sn, and 28.43 at.%Zn in the Mg-Zn-Sn system. This ternary reaction occurs in the Mg-4.5Zn-4.5Sn-2Al-based alloy due to the relatively higher Zn content, and the $Mg_{51}Zn_{20}$ phase is formed since water-cooling steel mold casting is typical of the non-equilibrium

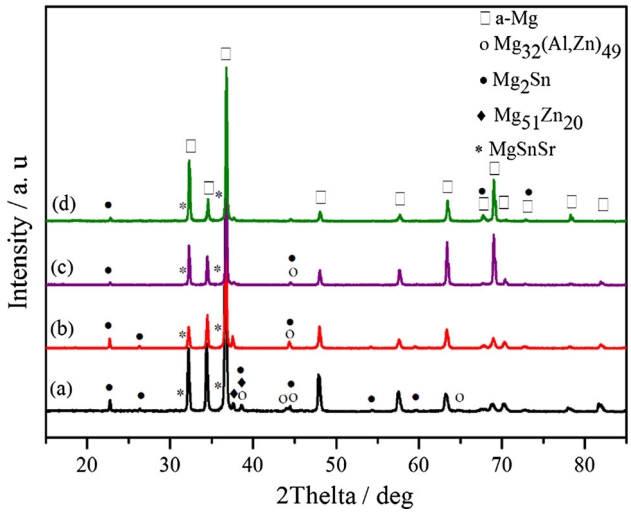

Fig. 1 The XRD patterns of the as-studied alloy in different states

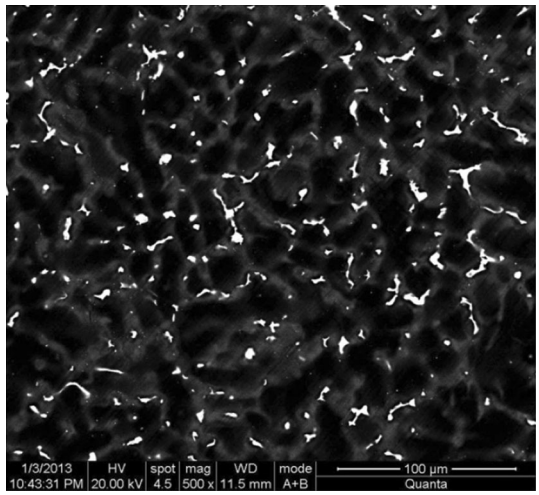

Fig. 2 The SEM image of the as-cast alloy

solidification. According to Harosh et al. (Ref 3), the DSC heating curve of the as-cast Mg-5.6%Sn-4.4%Zn-2.1%Al alloy is characteristic of three endo-thermal peaks, corresponding to the melting temperature of each phase, i.e., 348 °C for the eutectic reaction, 563 °C of Mg_2Sn, and 615 °C of the liquidus temperature. In combination with the XRD analysis, the endo-thermal peaks around 469 and 529 °C are possibly corresponding to the melting of the Mg_2Sn phase and the MgSnSr phase, respectively, which is uncertain at present and needs further confirmation in the future.

3.2 Solution-Treated Alloy

The intermetallics in the as-cast alloy have different melting points. Conventional single solution treatment is associated with the incomplete dissolution of most intermetallics or remelting. To achieve complete dissolution of the intermetallics and avoid remelting, the three-step solution treatment is adopted. The first step of 310 °C × 4 h is aimed at dissolving the non-equilibrium eutectics with the low melting point, the second step of 340 °C × 28 h is aimed at dissolving the $Mg_{51}Zn_{20}$ and the $Mg_{32}(Al, Zn)_{49}$ phases, while the third step of the high-temperature solution treatment is aimed at dissolving the Mg_2Sn and the MgSnSr phases. The mechanical properties of the as-cast and the solution-treated alloys are offered in Table 1.

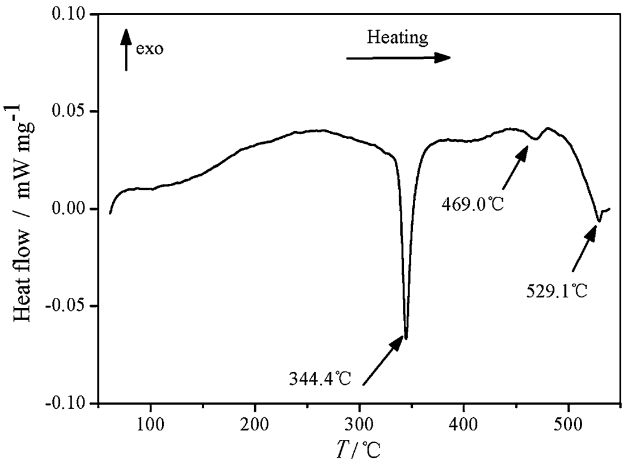

Fig. 3 The DSC heating curve of the as-cast alloy

3.2.1 Microstructure Evolution and Mechanical Property Change During 310 °C × 4 h + 340 °C × 28 h +420 °C × (0-6) h Solution Treatment. The OM images of the as-solutionized Mg-4.5Zn-4.5Sn-2Al-0.6Sr alloys that experience different solution treatments are shown in Fig. 4. As seen from Fig. 4(a), most of the grain-boundary compounds are dissolved in the α-Mg matrix and only a small quantity is still existent in the alloy that experiences a solution heat treatment of 310 °C × 4 h + 340 °C × 28 h. As indicated in Fig. 1(b), the diffraction peaks corresponding to the $Mg_{51}Zn_{20}$ and the $Mg_{32}(Al, Zn)_{49}$ phases are weakened in comparison with the as-cast alloy, indicating that the eutectics with low melting points are dissolved after the solution treatment of 310 °C × 4 h + 340 °C × 28 h. As seen from Fig. 4(b), a small amount of the intermetallics is residual in the alloy that experiences a solution heat treatment of 310 °C × 4 h + 340 °C × 28 h +420 °C × 2 h. A small portion is distributed along grain boundaries, while a relatively large portion is scattered within grains. As indicated in Fig. 1(c), the diffraction peaks corresponding to Mg_2Sn and MgSnSr are weakened in comparison with the alloy that experiences a solution heat treatment of 310 °C × 4 h + 340 °C × 28 h, indicating that both Mg_2Sn and MgSnSr are partially dissolved after the third step high-temperature solution treatment of 420 °C × 2 h. As seen from Fig. 4(c), almost all the intermetallics along grain boundaries are dissolved and a small portion of the intermetallics within grains is residual in the alloy that experiences a solution heat treatment of 310 °C × 4 h + 340 °C × 28 h +420 °C × 4 h. As seen from Fig. 4(d), all the intermetallics along grain boundaries are dissolved, a small amount of the fine dot-like second phase is residual within grains and an obvious grain growth is existent in the alloy that experiences a solution heat treatment of 310 °C × 4 h + 340 °C × 28 h +420 °C ×6 h. As indicated above, the intermetallics along grain boundaries become finer with the increasing solution time, while those within grains become granular and rounder.

The average grain size, the volume fraction of the residual second phases, the microhardness change, and the typical tensile curves versus the solution time are shown in Fig. 5. As seen from Fig. 5(a), the average grain size is almost constant with the solution time from 0 to 4 h at 420 °C, while it increases abruptly with the solution time of 6 h. The latter is about 86% larger than that of the two-step solution-treated alloy. In this sense, a prolonged solution time at 420 °C is not desirable. As seen from Fig. 5(b), the volume fraction of the residual second phases decreases sharply and the microhardness descends slightly with the increasing solution time from 0 to 4 h at 420 °C. In comparison with the two-step solution

Table 1 Mechanical properties of the as-cast and the solution-treated alloys

Alloy state	Mechanical properties			
	UTS/MPa	YTS/MPa	E_r/%	$HV_{0.1}$
As-cast	213	144	9.6	···
310 °C × 4 h + 340 °C × 28 h	206	137	11.2	63
310 °C × 4 h + 340 °C × 28 h + 420 °C × 2 h	210	140	12.1	62
310 °C × 4 h + 340 °C × 28 h + 420 °C × 4 h	216	142	11.7	62
310 °C × 4 h + 340 °C × 28 h + 420 °C × 6 h	202	131	10.2	60
310 °C × 4 h + 340 °C × 28 h + 440 °C × 2 h	218	145	11.3	65
310 °C × 4 h + 340 °C × 28 h + 460 °C × 2 h	238	150	12	65
310 °C × 4 h + 340 °C × 28 h + 460 °C × 4 h	203	131	9.3	60
310 °C × 4 h + 340 °C × 28 h + 480 °C × 2 h	172	117	7.1	61

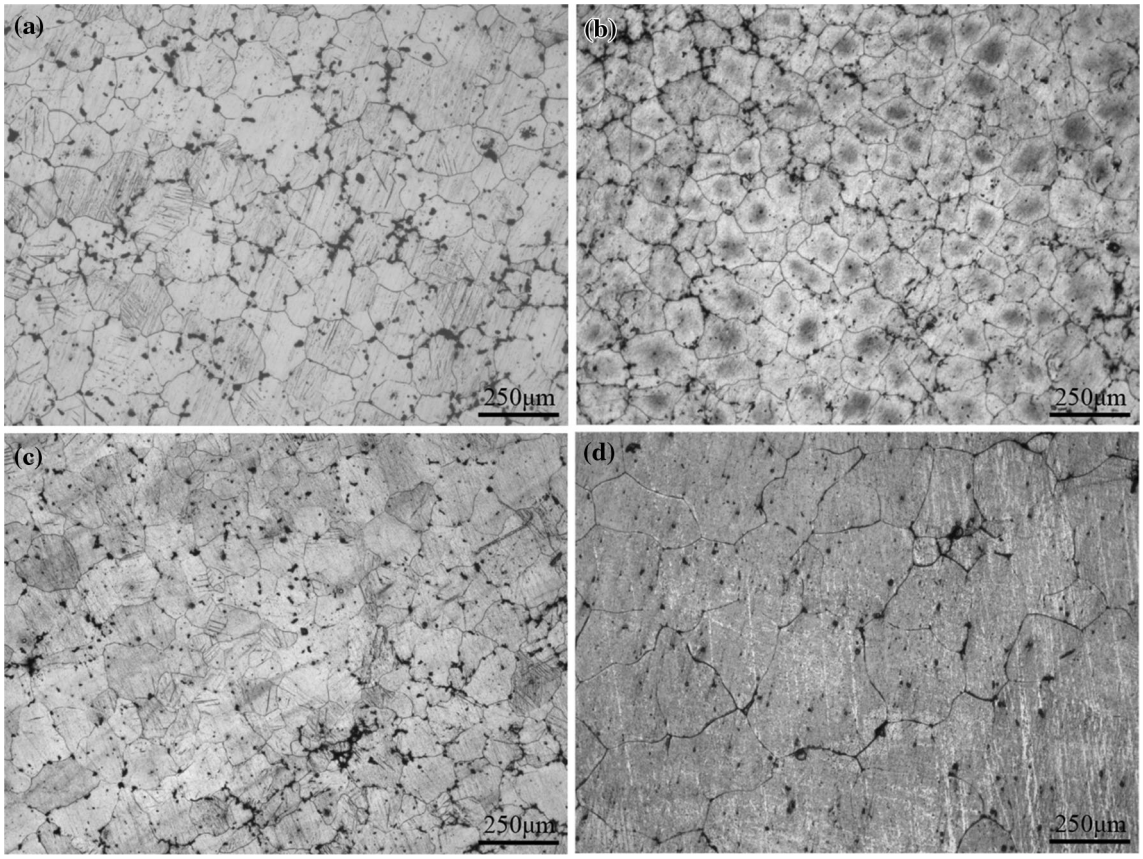

Fig. 4 The OM images of the solution-treated alloys with the different solution times

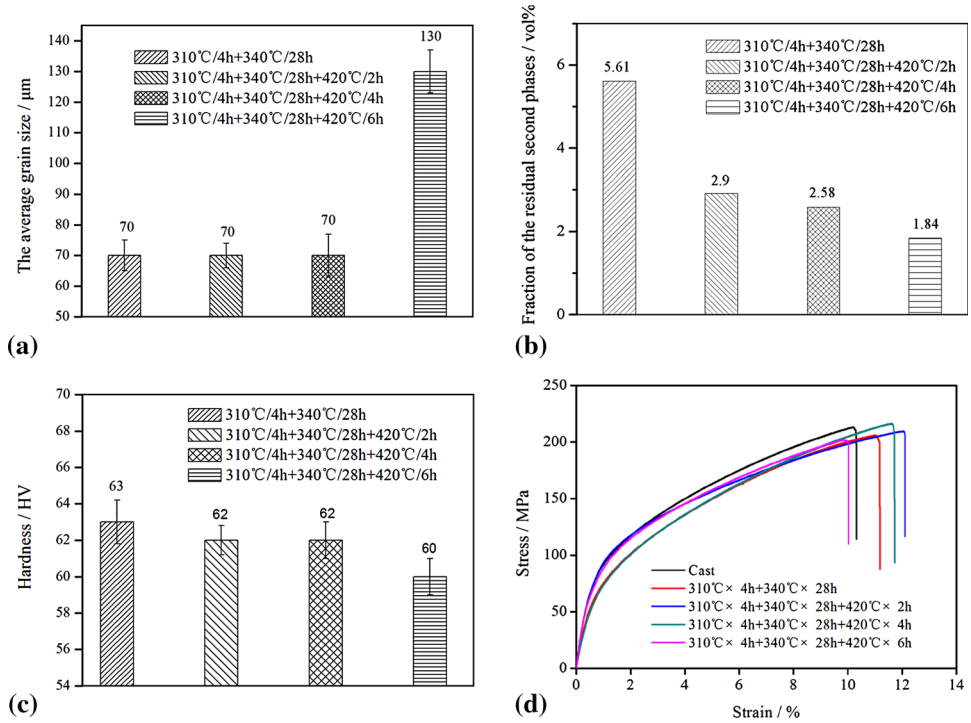

Fig. 5 The average grain size (a), the volume fraction of residual second phases (b), the microhardness change (c) and the typical tensile curves (d) versus the solution time

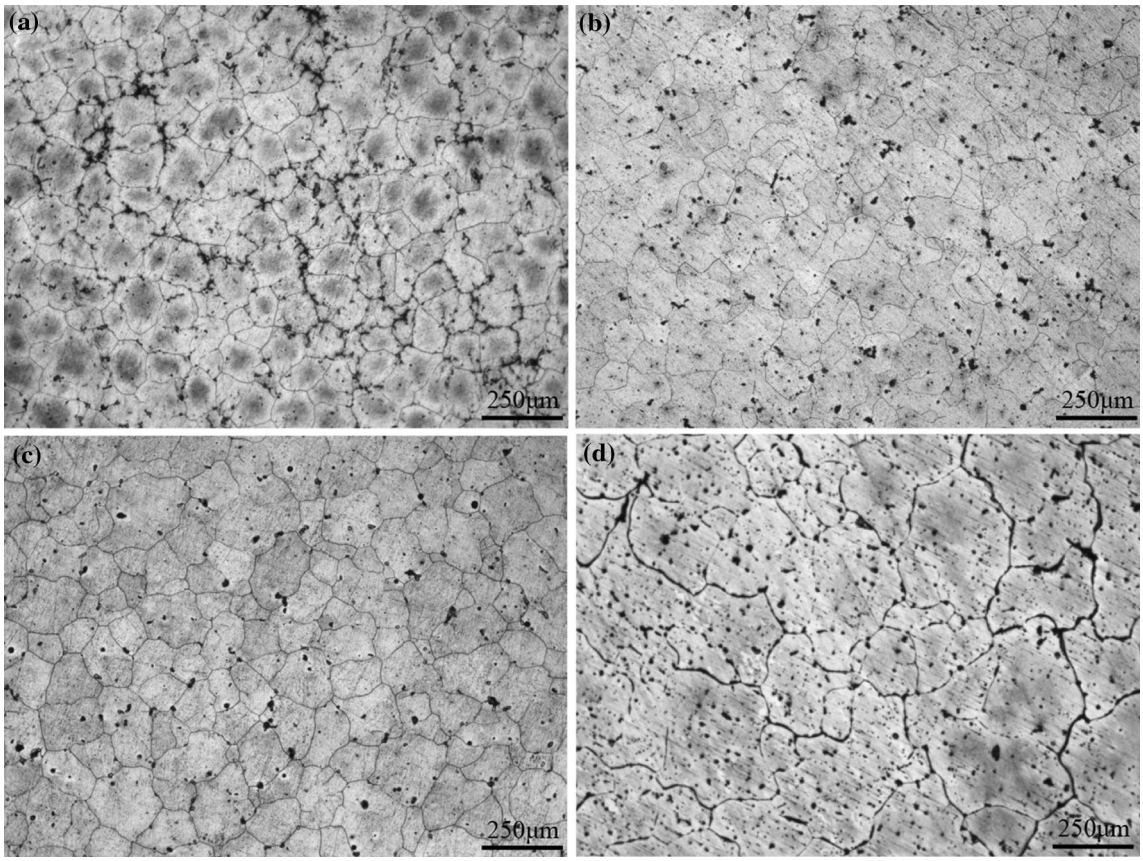

Fig. 6 The OM images of the solution-treated alloys with the different solution temperatures

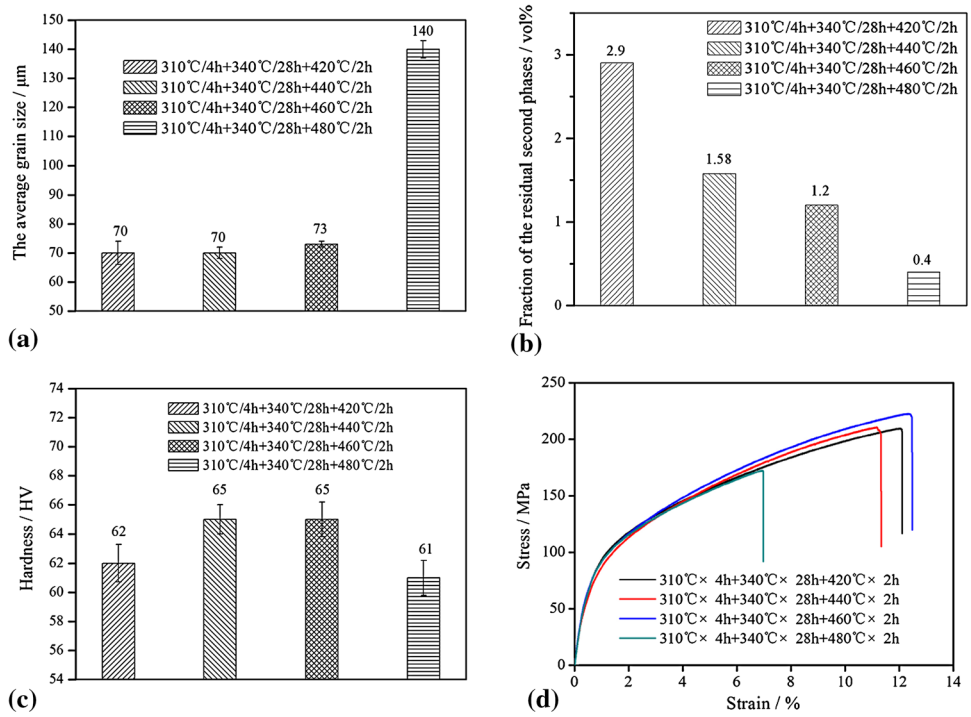

Fig. 7 The average grain size (a), the volume fraction of residual second phases (b), the microhardness change (c) and the typical tensile curves (d) versus the solution temperature

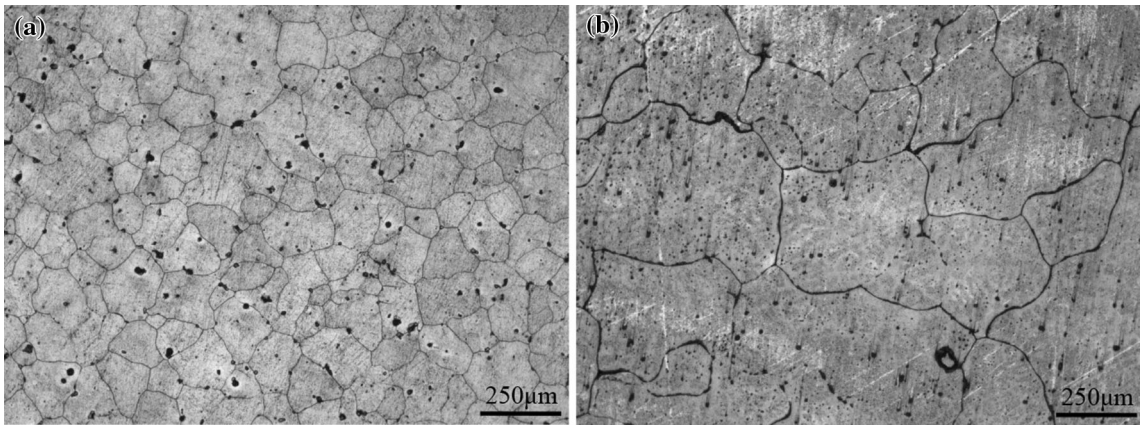

Fig. 8 The OM images of the solution-treated alloys

treatment, the volume fraction of the residual second phases in the alloy that experiences a solution heat treatment of 310 °C × 4 h + 340 °C × 28 h +420 °C × 2 h decreases from 5.61 to 2.9%, indicating that a high-temperature solution treatment at 420 °C is beneficial to the dissolution of the Mg_2Sn phase. A prolonged solution time at 420 °C brings about a slow decrease in the volume fraction of the residual second phases and the finer spheroidized second phase particles. Almost all the $Mg_{51}Zn_{20}$, the $Mg_{32}(Al, Zn)_{49}$ phases, and portion of the Mg_2Sn phase are dissolved and the enhanced solution strengthening of Zn, Sn, and Al atoms in the alloy is offset by the weakened second phase dispersion strengthening, resulting in the relatively constant microhardness of the solution-treated alloy. As seen from Fig. 5(c), with the increase of solution time from 4 h to 6 h at 420 °C, the microhardness decreases. As seen from Fig. 5(d) and Table 1, the UTS, the YTS, and the E_r values increase with the increase of solution time at first and then decrease with the solution time from 4 to 6 h at 420 °C. The former is possibly related to the enhanced solution strengthening, while the latter is possibly related to the severe grain coarsening. The alloy that experiences a solution heat treatment of 310 °C × 4 h + 340 °C × 28 h +420 °C × 4 h exhibits the best combined mechanical properties among the alloys solution treated at 420 °C, with the *UTS* of 216 MPa and the *Er* of 11.7%. Therefore, it is not desirable to improve the solutionizing effect by a prolonged solution time for the as-studied alloy.

3.2.2 Microstructure Evolution and Mechanical Property Change During 310 °C × 4 h + 340 °C × 28 h + (420-460) °C × 2 h Solution Treatment. The OM images of the as-solutionized Mg-4.5Zn-4.5Sn-2Al-0.6Sr alloys that experience different solution treatments are shown in Fig. 6. As seen from Fig. 6(a), a small amount of the intermetallics is residual in the alloy that experiences a solution heat treatment of 310 °C × 4 h + 340 °C × 28 h +420 °C × 2 h. A small portion is distributed along grain boundaries, while a relatively large portion is scattered within grains. As indicated in Fig. 1(c), both Mg_2Sn and MgSnSr are partially dissolved after the third step high-temperature solution treatment of 420 °C × 2 h. As seen from Fig. 6(b), almost all the intermetallics along grain boundaries are dissolved and a small portion of the intermetallics within grains is residual in the alloy that experiences a solution heat treatment of 310 °C × 4 h + 340 °C × 28 h + 440 °C × 2 h. The intermetallics along grain boundaries are granular and become finer, while those within grains become rounder. As seen from Fig. 6(c), almost all the intermetallics along grain boundaries are dissolved and only a minor portion of the intermetallics within grains is residual in the alloy that experiences a solution heat treatment of 310 °C × 4 h + 340 °C × 28 h + 460 °C × 2 h. As indicated in Fig. 1(d), the solution-treated alloy consists of three phases, i.e., α-Mg, Mg_2Sn, and MgSnSr. The diffraction peaks corresponding to the Mg_2Sn phase and the MgSnSr phase are relatively weak, indicating that their contents are rather low. Obviously, all the $Mg_{51}Zn_{20}$, the $Mg_{32}(Al, Zn)_{49}$ phases, and most of the Mg_2Sn phase are dissolved into the matrix. The residual intermetallics within grains are likely to be the MgSnSr phase or the mixture of Mg_2Sn and MgSnSr, which is reported in the literature (Ref 14) and is confirmed by the subsequent elemental mapping, EDS, and TEM analysis. As seen from Fig. 6(d), an obvious grain growth and the grain-boundary remelting are existent in the alloy that experiences a solution heat treatment of 310 °C × 4 h + 340 °C × 28 h + 480 °C × 2 h, indicating that 480 °C is too higher. As indicated above, the intermetallics along grain boundaries become granular with an increasing solution temperature, while those within grains become fine dot-like.

The average grain size, the volume fraction of the residual second phases, the microhardness change, and the typical tensile curves versus the solution temperature are shown Fig. 7. With the increase of solution temperature from 420 to 460 °C for 2 h, the average grain size and the *Er* value is almost constant, the volume fraction of the residual second phases decreases, and the microhardness, the UTS, and the YTS values increase. Almost all the $Mg_{51}Zn_{20}$, the $Mg_{32}(Al, Zn)_{49}$ phases,and portion of the Mg_2Sn phase are dissolved, and the effects of solution strengthening of Zn, Sn, and Al atoms in the alloy increase, resulting in the gradual increase in the microhardness, the UTS, and the YTS of the solution-treated alloy. With the increase of solution temperature from 460 to 480 °C for 2 h, the average grain size increases sharply, the volume fraction of the residual second phases decreases obviously, and the microhardness, the UTS, the YTS, and the E_r values descend quickly. Almost all the $Mg_{51}Zn_{20}$, the $Mg_{32}(Al, Zn)_{49}$, and the Mg_2Sn phases are dissolved, and the enhanced solution strengthening of Zn, Sn, and Al atoms in the alloy is offset and even overtaken by the weakened second phase dispersion strengthening and grain coarsening, resulting in the evident decrease of the microhardness and the tensile strength of the solution-treated alloy. Therefore, the high-temperature solution section in the three-step solution heat treatments should be limited below 480 °C. The alloy that experiences a solution heat treatment of

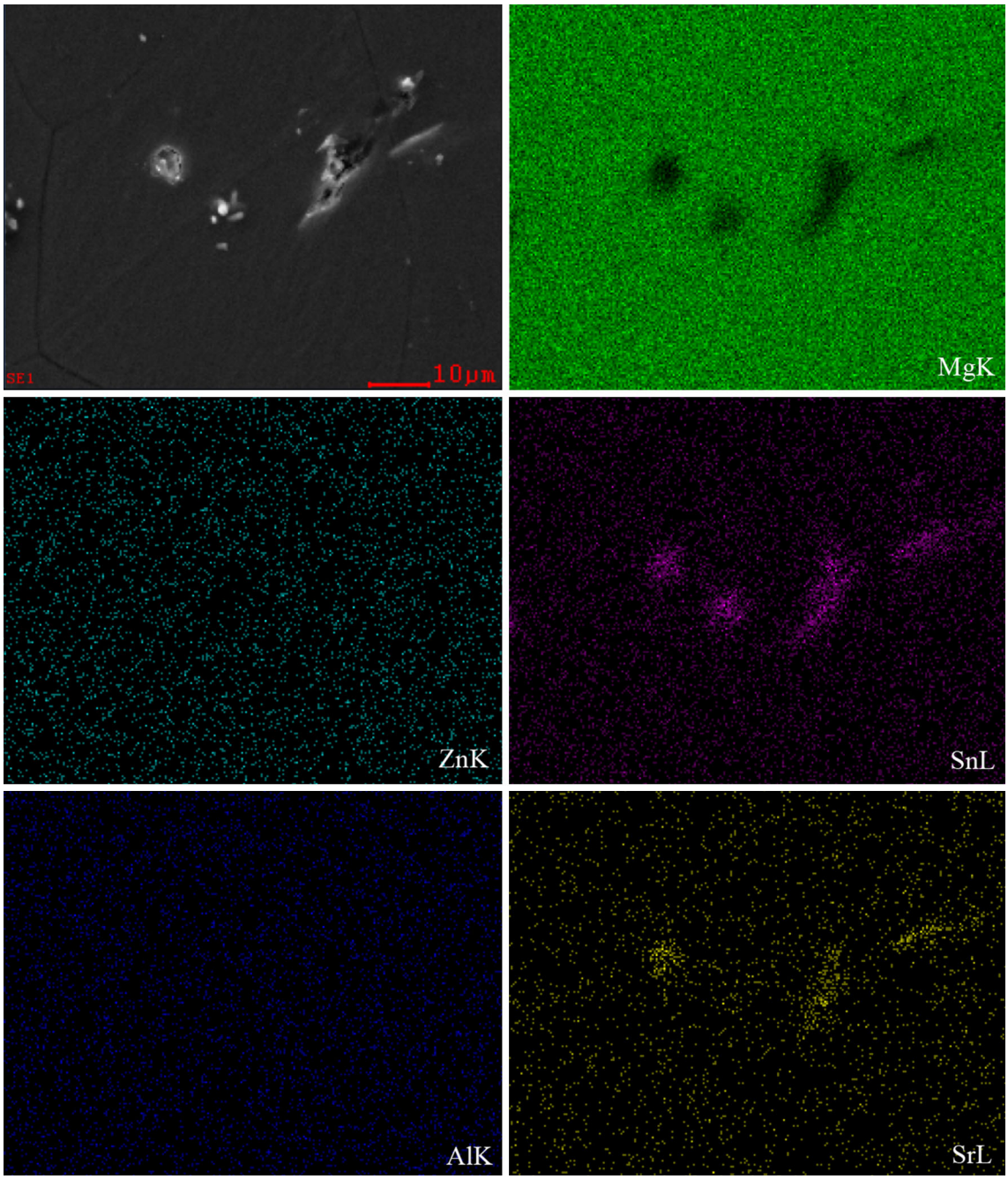

Fig. 9 The elemental mapping of the alloy solution treated at 310 °C × 4 h + 340 °C × 28 h + 460 °C × 2 h

310 °C × 4 h + 340 °C × 28 h + 460 °C × 2 h exhibits the best combined mechanical properties among all the as-studied alloys, with the *UTS* of 238 MPa and the *Er* of 12%, which are higher than that of 310 °C × 4 h + 340 °C × 28 h +420 °C × 4 h. In this sense, the solutionizing effect of 310 °C × 4 h + 340 °C × 28 h +460 °C × 2 h is much better than that of 310 °C × 4 h + 340 °C × 28 h +420 °C × 4 h. Obviously, the higher solution temperature is beneficial to the dissolution of the high-melting point phases i.e., Mg_2Sn and MgSnSr.

3.3 Determination of the Optimal Solution Treatment Conditions

The OM images of the as-solutionized Mg-4.5Zn-4.5Sn-2Al-0.6Sr alloys that experience a solution heat treatment of 310 °C × 4 h + 340 °C × 28 h followed by a high-temperature solution treatment at 460 °C are shown in Fig. 8. As seen from Fig. 8(a), all the $Mg_{51}Zn_{20}$, the $Mg_{32}(Al, Zn)_{49}$ phases, and most of the Mg_2Sn phase are dissolved into the matrix, while the MgSnSr phase and a minority of the Mg_2Sn phase are not dissolved after the solution heat treatment 310 °C × 4 h + 340 °C × 28 h + 460 °C × 2 h. As seen from Fig. 8(b), the alloy that experiences a solution heat treatment of 310 °C × 4 h + 340 °C × 28 h + 460 °C × 4 h exhibits the same microstructural features as that of 310 °C × 4 h + 340 °C × 28 h + 420 °C × 6 h. An obvious grain growth is existent and its average grain size is up to 150 μm. The *UTS* and the *Er* of the alloy that experiences a solution heat treatment of 310 °C × 4 h + 340 °C × 28 h + 460 °C × 4 h are 203 MPa

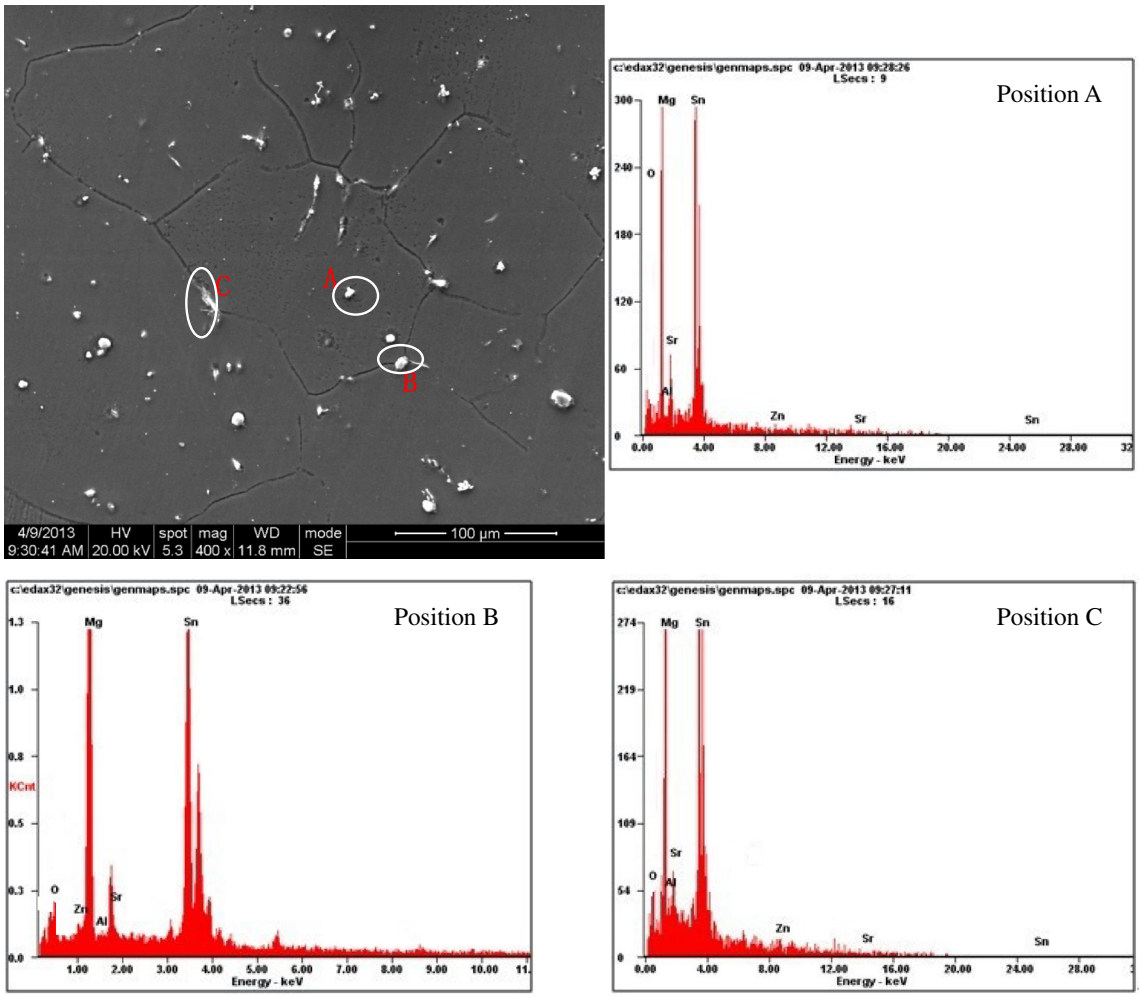

Position	Chemical compositions (at%)				
	Zn	Al	Sn	Sr	Mg
A	2.2	0.8	27.2	4.4	65.4
B	1.5	0.4	19.2	1.8	77.1
C	2.1	1.3	17.6	1.3	77.7

Fig. 10 The SEM image and the EDS analysis of the certain intermetallics in the alloy solution treated at 310 °C × 4 h + 340 °C × 28 h + 460 °C × 2 h

and 9.3%, respectively, which are much lower than the alloy that experiences a solution heat treatment of 310 °C × 4 h + 340 °C × 28 h + 460 °C × 2 h. Therefore, the high-temperature solution section at 460 °C should be limited below 4 h. On the basis of the data mentioned above, the optimal solution treatment for the Mg-4.5Zn-4.5Sn-2Al-0.6Sr alloy is 310 °C × 4 h + 340 °C × 28 h + 460 °C × 2 h since the dissolution of most intermetallics and no obvious grain growth are involved.

As seen from Fig. 1(d), the alloy that experiences a solution heat treatment 310 °C × 4 h + 340 °C × 28 h + 460 °C × 2 h consists of three phases, i.e., α-Mg, Mg_2Sn, and MgSnSr. Almost all the $Mg_{51}Zn_{20}$, the $Mg_{32}(Al, Zn)_{49}$ phases, and most of the Mg_2Sn phase are dissolved into the matrix. The elemental mapping and the SEM images of the alloy solution treated at 310 °C × 4 h + 340 °C × 28 h + 460 °C × 2 h are shown in Fig. 9 and 10, respectively. As seen from Fig. 9, the residual intermetallics within grains in the solution-treated alloy are rich in Mg, Sn, and Sr, indicating that the MgSnSr phase and a minority of the Mg_2Sn phase are not dissolved. To clarify the residual intermetallics, the further SEM examination and the

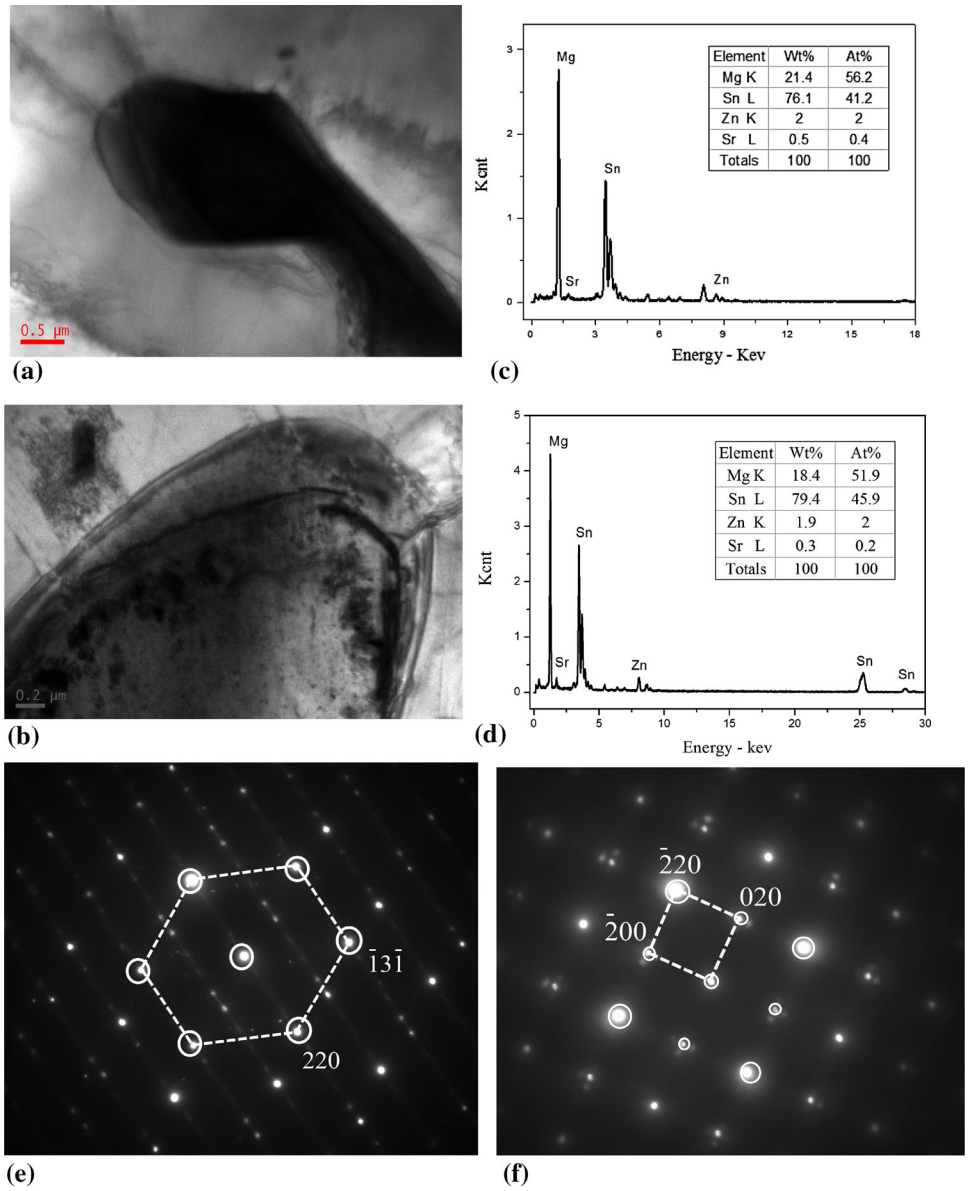

Fig. 11 The TEM images of the bone-like phase after solution treatment (a, b), the corresponding EDS results (c, d) and the SAED patterns (e, f)

TEM study are conducted. As seen from Fig. 10, the residual intermetallics are rich in Sn and contain a certain amount of Sr, indicating they are the Mg_2Sn phase dissolved with Sr or the mixture of Mg_2Sn and MgSnSr. Moreover, the intermetallics within the grains have a higher Sr content than those along grain boundaries. The former is likely to be the mixture of Mg_2Sn and MgSnSr, while the latter is possibly to be the Mg_2Sn phase dissolved with Sr. It is confirmed by the successive TEM analysis.

As shown in Fig. 11(a-d), the bone-like particles with the size of 3-5 μm are detected, with the atomic ratios of Mg to Sn around 1.3 and containing a little Sr (0.3-0.5 wt.%). As seen form Fig. 11(e) and (f), the bone-like phase is confirmed to be the Mg_2Sn phase with a little Sr. As shown in Fig. 12, the large spheroid phase with the size of about 3 μm is detected, containing a relatively high Sr element up to 9.9 wt.% and with the atomic ratio of Mg to Sn about 1.25. Its Sr content is much higher than the bone-like phase. According to the literature (Ref 16), no Mg-Sn-Sr ternary phase diagram is reported and the Mg_2Sn phase shows no solubility with other elements in the Mg-Al-Ca-Mn-Sn-Sr alloy system. From this, it is speculated that the large spheroid phase is likely to be the MgSnSr phase or the mixture of Mg_2Sn and MgSnSr. To further confirm this, the SAED pattern of this phase is shown in Fig. 12(c) and the MgSnSr phase is determined. The *UTS* and the *Er* of the as-solutionized alloy are 238 MPa and 12%, respectively, while those of the as-cast alloy are 213 MPa and 9.6%, respectively.

4. Discussion

Solution heat treatment (T4) causes the dissolution of the second phases in the Mg-Zn-Sn alloys and aims at obtaining the α-Mg supersaturated solid solution for successive aging. Optimization of T4 treatment parameters is of great significance especially for the alloy system involved with two or more kinds of

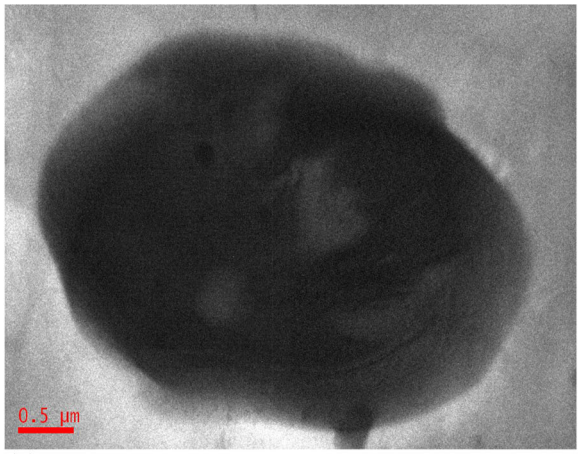

(a)

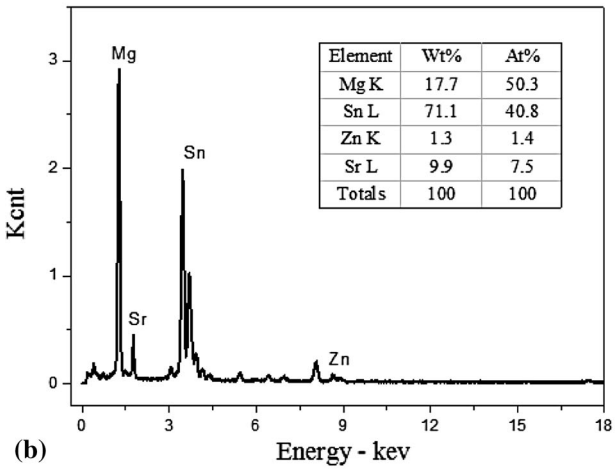

(b)

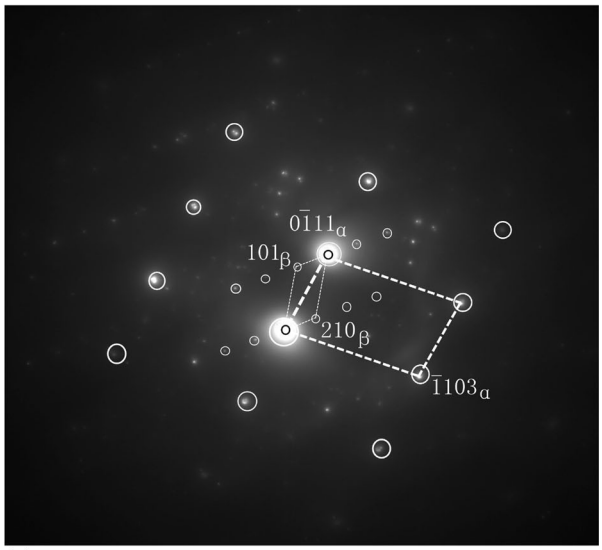

(c)

Fig. 12 The TEM image of the large spheroid thermal stable phase after solution treatment (a), the corresponding EDS result (b) and the SAED pattern (c)

the second phases, which show great differences in the melting point. Complete dissolution of the second phases into the matrix as possible and no obvious grain growth are the two prerequisites. Therefore, the heat treatment temperature should be high enough to enhance the kinetics of phase transformation, but low enough to prevent or slow down the grain growth. Moreover, a prolonged solution time is also beneficial to atomic diffusion and thus promotes the dissolution of the second phases.

As far as the as-cast Mg-4.5Zn-4.5Sn-2Al-0.6Sr alloy is concerned, four kinds of the intermetallic phases i.e., $Mg_{51}Zn_{20}$, $Mg_{32}(Al, Zn)_{49}$, Mg_2Sn, and MgSnSr are involved. Their melting points are 347, 535, and 770 °C, respectively, except for MgSnSr. As mentioned above, the morphologies of the second phases can be modified during the solution heat treatment. After the two-step solution heat treatment (310 °C × 4 h + 340 °C × 28 h), the continuous network-like $Mg_{51}Zn_{20}$, $Mg_{32}(Al, Zn)_{49}$ phases are broken into the disconnected and then are completely dissolved. With the prolonged solution time and the increasing temperature, the bone-like Mg_2Sn phase is fragmentized into the island-like and some particles are spheroidized, while the compounds with a relatively high Sr element are still remained.

Accompanied with the slow dissolution of Mg_2Sn at grain boundaries, the second phases decrease and their restriction effect on grain-boundary migration gradually vanishes during solution treatment at the relatively low temperature. Therefore, severe grain coarsening occurs with a prolonged solution time up to 6 h at 420 °C. The higher solution treatment temperature is beneficial to atomic diffusion along both grain boundaries and phase interfaces due to the relatively high vacancy concentration and thus the faster dissolution of Mg_2Sn into the matrix is achieved. No obvious grain-boundary migration occurs since the solution time is relatively short, and thus, the grain size is constant even after the high-temperature short-time solution treatment of 460 °C × 2 h. On the other hand, the diffusion constants of Zn, Al, and Sn in Mg are 4.1×10^{-1}, 1.53×10^{-1}, and 4.27 m^2/s, respectively, while their activation energies of diffusion are 120, 125, and 150 KJ/mol respectively (Ref 17). Obviously, the diffusion coefficient of Sn in Mg is rather low and the dissolution of the Sn-containing phases is relatively difficult. However, the temperature rise brings about an obvious increase in the diffusion coefficient of Sn in Mg since its activation energy of diffusion is much higher than that of Zn in Mg. The diffusion coefficients of Sn in Mg at 340, 420, and 480 °C are about 7.28×10^{-13}, 1.62×10^{-11}, and 1.68×10^{-10} m^2/s, respectively. Hence, the volume fraction of the residual second phase decreases obviously with the increase of solution temperature from 420 to 480 °C for 2 h.

As shown in Fig. 12, the large spheroid phase is the residual MgSnSr phase in the alloy that experiences the solution treatment of 310 °C × 4 h + 340 °C × 28 h + 460 °C × 2 h. It has been reported that the appearance of the relatively high Sr content in the compound containing Mg and Sn may lead to the formation of the MgSnSr phase (Ref 14, 18). The dissolution of MgSnSr in the matrix is rather slow since the volume diffusion of Sn and Sr in Mg is involved. Moreover, the MgSnSr phase has a relatively high melting point and thus exhibits a relatively high thermal stability. Therefore, complete dissolution of MgSnSr in the matrix through the three-step solution heat treatment is rather difficult.

However, the *UTS* and the *Er* of the alloy solution treated at 310 °C × 4 h + 340 °C × 28 h + 460 °C × 2 h are 238 MPa and 12%, respectively, which are 25 MPa and 2.4% higher than the as-cast alloy, respectively. The alloy solution treated at 310 °C × 4 h + 340 °C × 28 h + 460 °C × 2 h exhibits an improved combination of strength and ductility, which is associated with a fine grain size and the relatively uniform distribution of the residual second phases. It is reported that the

Tx treatment offers an improved combination of strength and ductility for the AZ91D alloy (Ref 19). T_x is carried out at an intermediate temperature close to the solvus (370 °C) for a much shorter length of time, causing partial dissolution of the non-equilibrium β phase, breaking up the β network and thus resulting in a composite structure. The comparative study on mechanical properties of the aged state is being taken. Maybe, it can also provide a new heat treatment schedule to achieve an optimal combination of mechanical properties in the Mg-Zn-Sn alloys.

5. Conclusions

(1) The intermetallics along grain boundaries become finer with an increasing solution time from 0 to 6 h during the solution section of 420 °C, while those within grains become granular and rounder. A prolonged solution time is not desirable for the as-studied alloy.

(2) The intermetallics along grain boundaries become granular with an increasing solution temperature from 420 to 480 °C during the isochronic solution heat treatment of 2 h, while those within grains become fine dot-like. A higher solution temperature is beneficial to the dissolution of the high-melting point phases, i.e., Mg_2Sn and MgSnSr.

(3) The optimal solid solution condition for the Mg-4.5Zn-4.5Sn-2Al-0.6Sr alloy is 310 °C × 4 h + 340 °C × 28 h + 460 °C × 2 h since the dissolution of most intermetallics and no obvious grain growth are involved, and the alloy exhibits the highest strength and the best plasticity among all the solution-treated alloys. The UTS and the elongation to rupture of the solution-treated alloy are 238 MPa and 12%, respectively, about 25 MPa and 2.4% higher than the as-cast alloy respectively.

(4) The residual second phases after the optimal solution treatment are confirmed to be the Mg_2Sn phase and the MgSnSr phase with a relatively high thermal stability and exhibit a relatively uniform distribution in the matrix, contributing to the improved combination of strength and ductility.

Acknowledgments

The authors are grateful to the support of the Natural Science Foundation Project of China (51001046, 51274092), the National Research Foundation for the Doctoral Program of Higher Education of China (20120161110040), and the Young Teacher Growth Fund of Hunan University (531107021095).

References

1. G.Y. Yuan, M.P. Liu, W.J. Ding et al., Microstructure and Mechanical Properties of Mg-Zn-Si Based Alloys, *Mater. Sci. Eng. A*, 2003, **357**, p 314–320
2. T.T. Sasaki, J.D. Ju, K. Hono et al., Heat-Treatable Mg-Sn-Zn Wrought Alloy, *Scripta Mater.*, 2009, **61**, p 80–83
3. S. Harosh, L. Miller, G. Levi et al., Microstructure and Properties of Mg-5.6%Sn-4.4%Zn-2.1%Al Alloy, *J. Mater. Sci.*, 2007, **42**, p 9983–9989
4. T.T. Sasaki, K. Yamamoto, T. Honma, S. Kamado, and K. Hono, A High-Strength Mg-Sn-Zn-Al Alloy Extruded at Low Temperature, *Scripta Mater.*, 2008, **59**, p 1111–1114
5. W.L. Xiao, S.S. Jia, J.L. Wang et al., The Influence of Mischmetal and Tin on the Microstructure and Mechanical Properties of Mg-6Zn-5Al-Based Alloys, *Acta Mater.*, 2008, **56**(5), p 934–941
6. M.B. Yang and F.S. Pang, Effects of Sn Addition on As-Cast Microstructure, Mechanical Properties and Casting Fluidity of ZA84 Magnesium Alloy, *Mater. Des.*, 2010, **31**(1), p 68–75
7. J.H. Chen, Z.H. Chen, H.G. Yan et al., Effects of Sn Addition on Microstructure and Mechanical Properties of Mg-Zn-Al Alloys, *J. Alloy Compd.*, 2008, **461**(1–2), p 209–215
8. M.B. Yang, L. Cheng, and F.S. Pan, Effects of Calcium Addition on As-Cast Microstructure and Mechanical Properties of Mg-5Zn-5Sn Alloy, *Trans. Nonferr. Met. Soc. China*, 2010, **20**, p 769–775
9. S. Cohen, G.R. Goren-Muginstein, S. Avraham et al., Phase Formation, Precipitation and Strengthening Mechanisms in Mg-Zn-Sn and Mg-Zn-Sn-Ca Alloys, *Magnesium Technology*, A.A. Luo, Ed., TMS, Warrendale, PA, 2004, p 301–305
10. A. Gorny, M. Bamberger, and A. Katsman, High Temperature Phase Stabilized Microstructure in Mg-Zn-Sn Alloys with Y and Sb Additions, *J. Mater. Sci.*, 2007, **42**, p 10014–10022
11. W.N. Tang, S.S. Park, and B.S. You, Effect of the Zn Content on the Microstructure and Mechanical Properties of Indirect-Extruded Mg-5Sn-*x*Zn Alloys, *Mater. Des.*, 2011, **32**, p 3537–3543
12. H.-T. Son, D.-G. Kim, and J.S. Park, Effects of Ag Addition on Microstructures and Mechanical Properties of Mg-6Zn-2Sn-0.4Mn-Based Alloy System, *Mater. Lett.*, 2011, **65**, p 3150–3153
13. X.Q. Pan, J.H. Chen, H.G. Yan, B. Su, J.Y. Wei, and C. Fan, Effects of the Zn/Sn Mass Ratio on Microstructure and Mechanical Properties of the Mg-Zn-Sn-Al-Ca Alloys, *Mater. Sci. Technol. Lond.*, 2013, **29**(2), p 169–176
14. X. He, J.H. Chen, H.G. Yan, B. Su, G.H. Zhang, and C.M. Miao, Effects of Minor Sr Addition on Microstructure and Mechanical Properties of the As-Cast Mg-4.5Zn-4.5Sn-2Al-Based Alloy System, *J. Alloy Compd.*, 2013, **579**, p 39–44
15. P. Ghosh, M. Mezbahul-Islam, and M. Medraj, Critical Assessment and Thermodynamic Modeling of Mg-Zn, Mg-Sn, Sn-Zn and Mg-Sn-Zn Systems, *Calphad*, 2012, **36**, p 28–43
16. J. Gröner, A. Janz, A. Kozlov, D. Mirković, and R. Schmid-Fetzer, Phase Diagrams of Advanced Magnesium Alloys Containing Al, Ca, Sn, Sr and Mn, *JOM*, 2008, **60**(12), p 32–38
17. Z.H. Chen, *Creep Resistant Magnesium Alloy*, Chemical Industry Press, Beijing, 2007, p 431–459
18. H.M. Liu, Y.G. Chen, H.F. Zhao, S.H. Wei, and W. Gao, Effects of Strontium on Microstructure and Mechanical Properties of As-Cast Mg-5 wt.%Sn alloy, *J. Alloy Compd.*, 2010, **504**(2), p 345–350
19. Y. Wang, G. Liu, and Z. Fan, A New Heat Treatment Procedure for Rheo-Diecast AZ91D Magnesium Alloy, *Scripta Mater.*, 2006, **54**, p 903–908